Recipes for Writing Algorithms for Atmospheric Corrections and Temperature/Emissivity Separations in the Thermal Regime for a Multi-Spectral Sensor

Christoph C. Borel and William Clodius
Space and Remote Sensing Sciences Group
Mail Stop C 323, Los Alamos National Laboratory
Los Alamos, NM 87545, USA

ABSTRACT

This paper discusses the algorithms created for the Multi-spectral Thermal Imager (MTI) to retrieve temperatures and emissivities. Recipes to create the physics based water temperature retrieval, emissivity of water surfaces are described. A simple radiative transfer model for multi-spectral sensors is developed. A method to create look-up-tables and the criterion of finding the optimum water temperature are covered. Practical aspects such as conversion from band-averaged radiances to brightness temperatures and effects of variations in the spectral response on the atmospheric transmission are discussed. A recipe for a temperature/emissivity separation algorithm when water surfaces are present is given. Results of retrievals of skin water temperatures are compared with in-situ measurements of the bulk water temperature at two locations are shown.

Keywords: MTI, Multi-spectral Imaging, Water Temperature, Emissivity, Atmospheric Correction

1. Introduction

In the solar reflective region it is very common to perform atmospheric corrections based on dark targets such as water or vegetation to obtain surface reflectances which can be used to perform material identification tasks. In the thermal we have the difficulty of retrieving not only the emissivity=1-reflectance but also the surface temperature, which is called temperature emissivity separation or TES. Many algorithms have been devised to perform TES based on statistical properties of natural emissivities, e.g. correlations of the range of emissivities in a spectral range to the maximum emissivity for instruments such as ASTER, MODIS and TIMS. The data from ASTER, for example is being atmospherically corrected using not the data from the sensor itself but uses other sensors data such as MODIS or weather assimilation data with resolutions of 1 by 1 degrees. In this paper we show how the Multi-spectral Thermal Imager (MTI) takes advantage of two water vapor sensitive channels out of five in total to retrieve atmospheric temperature and water vapor over surfaces with known emissivities such as water to perform an in-scene atmospheric correction of multi-spectral thermal data. The algorithms will be described so that they can easily be adapted to other multi-spectral thermal sensors.

2. Recipe for a physics based water temperature retrieval

The physics based retrieval of water temperatures is based on two observations:

1. The problem of temperature-emissivity separation which usually requires solving for $(N+1)$ unknowns can be simplified in the case of a known surface emissivity, such as water, to solving for the temperature only. Note that in reality an additional atmospheric correction needs to be performed which requires knowledge of the atmospheric parameters such as columnar water vapor and atmospheric temperature.
2. A correct solution of (1) through an atmospheric correction of the sensor radiance should lead to the same skin temperature for all multi-spectral channels using the same atmospheric parameters.

Further author information: (Send correspondence to C.C.B.)
C.C.B.: E-mail: cborel@lanl.gov; WEB: nis-www.lanl.gov/~borel; Telephone: (505) 667-8972; Fax: (505) 667-3815
W.C.: E-mail: wclodius@lanl.gov

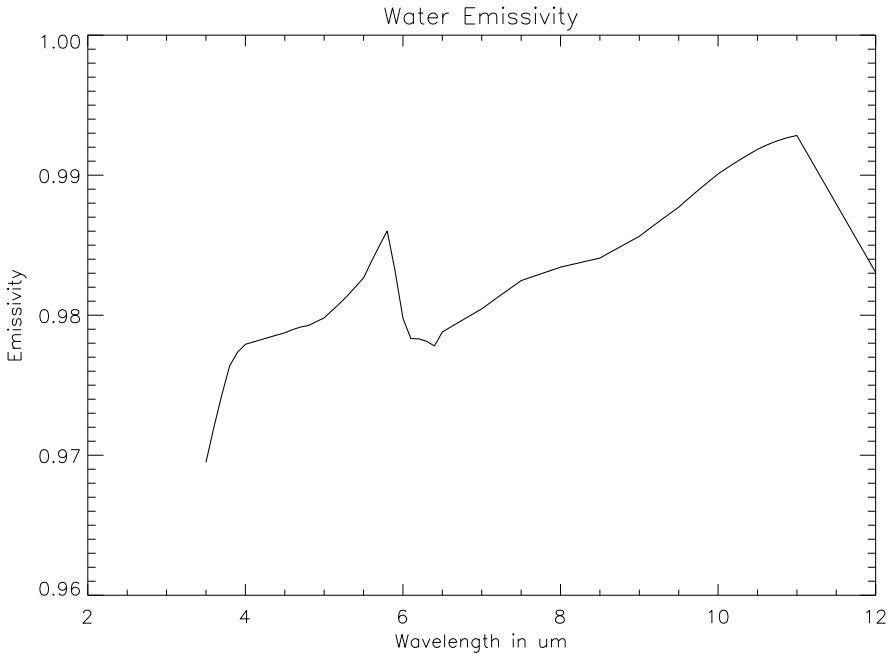

Figure 1. Emissivity of water for a view zenith of 10 degrees

2.1. Recipe for an emissivity model for water surfaces

The emissivity of water can be computed using a number of different models. For this paper we used an implementation by Henderson (unpublished 1995) which is based on the classic Cox-Munk model (1954) which is fine for small view zenith angles. For larger view angles, more sophisticated models should be used which take polarization and shadowing effects into account (e.g. Theiler and Henderson, (1997), Henderson et al, (2001)) and usually are based on Monte Carlo raytracing simulations of simulated sea surfaces (e.g. Pierson and Moskowitz (1964), Preisendorfer and Mobley, (1986)). Henderson's code uses measured and imaginary refractive indices by Irvine and Pollack (1968) with a correction for the erroneous entry at 4.66 μm for the imaginary part in the original paper. This emissivity model can compute the emissivity as a function of wavelength, view zenith, relative azimuth between view and wind direction and wind speed (up to 14 m/s). Figure 1 shows the emissivity spectrum for a range from 3.5 to 13 μm.

2.2. A simple radiative transfer model for multi-spectral sensors

The physics based water temperature retrieval was introduced in Borel et al (1999) and has since been applied in a revised form to data from the Multi-spectral Thermal Imager (MTI) which was launched in March of 2000. The revised form uses a look-up-table (LUT) of MODTRAN computed band averaged transmissions as a function of columnar water vapor rather than the non-linear fit used in the 1999 paper.

From radiative transfer for the thermal regime, the measured spectral radiance $L_{m,\lambda}(H)$ along a ray reaching the sensor at height H and wavelength λ is:

$$L_{m,\lambda}(H) = L_\lambda(\text{surface}) + L_\lambda(\text{path}) + L_\lambda(\text{reflected downwelling}) \quad (1)$$
$$= \varepsilon_{w,\lambda} B_\lambda(T_w)\tau_\lambda + \int_0^H B_\lambda(T_a(z))\kappa_\lambda(z)dz + (1-\varepsilon_{w,\lambda})\tau_\lambda \int_H^0 B_\lambda(T_a(z))\kappa_\lambda(z)dz,$$

where $\varepsilon_{w\lambda}$ is the water emissivity and $B_\lambda(T)$ is the Planck function in units of $W/(m^2 \mu m\ sr)$. T_w is the skin temperature and $T_a(z)$ is the atmospheric temperature profile. The atmospheric transmission is τ_λ and $\kappa_\lambda(z) = (\delta\tau_\lambda(z))/(\delta z)$. The following assumptions simplify further derivations:

1. We neglect the reflected down-welling radiance of the atmosphere. The radiance is small in spectral bands with good atmospheric transmission and water surfaces reflect less than 3 %.

2. For simplicity we assume a one-layer model where $\kappa_\lambda(z) = \kappa_{0,\lambda} \rightarrow \tau_\lambda = \kappa_{0,\lambda} H$ and $T_a(z) = const$ which we'll call the effective atmospheric temperature. The path radiance can be approximated by: $L_\lambda(path) = B_\lambda(T_a)[1 - \tau_\lambda(CW)]$, where CW is the columnar water vapor amount. This approximation is quite good in atmospheric windows and its validity was tested using MODTRAN for MTI's spectral channels which lie in atmospheric window regions.

With these assumptions the measured radiance at wavelength λ is:

$$L_{m,\lambda} = \varepsilon_{w,\lambda} B_\lambda(T_w)\tau_\lambda(CW) + B_\lambda(T_a)[1 - \tau_\lambda(CW)]. \quad (2)$$

Solving eq(2) for the skin temperature T_w we find:

$$T_w = B_\lambda^{-1}\left[\frac{L_{m,\lambda} - B_\lambda(T_a)[1 - \tau_\lambda(CW)]}{\varepsilon_{w,\lambda}\tau_\lambda(CW)}\right], \quad (3)$$

where the function B^{-1} is the inverse Planckian. For a multi-spectral instrument we need to integrate eq (3) over a range of wavelengths which results in:

$$T_w = B_i^{-1}\left[\int_{\lambda(i)_a}^{\lambda(i)_b} \frac{L_{m,\lambda} - B_\lambda(T_a)[1 - \tau_\lambda(CW)]}{\varepsilon_{w,\lambda}\tau_\lambda(CW)} d\lambda\right], \quad (4)$$

where B_i^{-1} is an inverse Planckian for channel i. Unfortunately the integral equation (4) is impossible to solve accurately because in a multi-spectral sensor we do not measure the sensor radiance as a function of wavelength. Furthermore we assumed in eq (4) that the spectral response R_λ is unity between the wavelength range given by $\lambda(i)_a$ to $\lambda(i)_b$. In reality the spectral response R_λ is the product of the detector response D_λ and filter function F_λ. Thus an approximation of eq (4) is necessary to break the integral into two parts, one for the numerator and one for the denominator:

$$T_w = B_i^{-1}\left[\frac{L_{m,i} - \int B_\lambda(T_a)[1 - \tau_\lambda(CW)d\lambda]}{\int \varepsilon_{w,\lambda}\tau_\lambda(CW)d\lambda}\right]. \quad (5)$$

2.3. Building a look-up-table using MODTRAN

The algorithm uses MODTRAN results for the 6 standard atmospheres in MODTRAN (tropical, mid-latitude summer, mid-latitude winter, sub-arctic summer, sub-arctic winter and 1976 US standard), 3 altitudes (sea level, 1000 m and 2000 m), 4 view zenith angles (nadir, 10 deg, 20 deg and 60 deg) and up to 19 columnar water vapor (CW) amounts from 0.1 to 8 g/cm^2. These variations result in hundreds of individual MODTRAN runs.

To vary the water vapor amount we make use of a relatively unknown feature in MODTRAN 3.7 and 4 which was pointed out to us by Prof. David Archer, University of Chicago. A very nice interactive simulation demonstrating this feature can be found at: *http://geosci.uchicago.edu/~archer/cgimodels/radiation.html*. The water vapor scaling is only documented in the code itself and allows the scaling of CW in the FORTRAN routine `SCLCOL.f` over a range of values. To access this feature a simple additional entry on the second line of `TAPE5` is required after the CO2 amount, e.g. `F 0F 2 370.000 G2.250` which scales the CW to 2.25 g/cm^2 denoted by the letter "G". Using the letter "A" the CW can be specified in $atm - cm$. Without any letter the number is interpreted as a scaling factor. In the case that the scaled water vapor amount results in an un-physical situation, e.g. a higher than 100 % relative humidity `TAPE6` will not contain an output statement with the final scaled value, e.g. `FINAL: 2.25000 GM / CM2`. However one of the most important variables the atmospheric temperature profile has not been varied yet.

Two separate runs are made at 1 cm^{-1} sampling (2 cm^{-1} resolution) from 3.3-5.2 μm in the mid-wave IR and 7.5-11 μm in the long-wave IR. To reduce access time for future processing and storage requirements the output files from MODTRAN (tape7) are read and a table of the total transmission as a function of wavenumber and water vapor is generated for each run for a specific atmosphere type, altitude and view zenith angle.

To vary the atmospheric temperature we used the approximation shown in eq (2) which we verified for MODTRANs standard atmospheres using the following steps:

1. Compute the path radiance with MODTRAN for a given view geometry,
2. Fit an atmospheric temperature to computed path radiance, and
3. Compare the result of the band-averaged radiance from the MODTRAN run with the approximation to $L_i(path)$ from eq. (2).

2.4. Look-up-table generation

The look-up-table for the atmospheric correction is computed for each of the 6 atmospheres, 3 heights, 4 view angles and up to 19 water vapor amounts using the following steps:

1. Read the spectral emissivity data ε_λ,
2. Read the spectral response data $R_\lambda(i)$ for all thermal channels i and normalize the integral over R_λ to unity:
$$R^*_\lambda = \frac{R_\lambda}{\int_{\lambda(i)_a}^{\lambda(i)_b} R_\lambda d\lambda},$$
3. Read the MODTRAN derived spectral transmission τ_λ,
4. Interpolate the spectral emissivity to the same wavelength grid as the transmission,
5. Numerically integrate the products over each filter band i for a columnar water vapor amount CW:
   (a) where the average transmission in band i is:
$$\tau_i(CW) = \int_{\lambda(i)_a}^{\lambda(i)_b} R^*_\lambda \tau_\lambda(CW) d\lambda,$$
   (b) where the average of emissivity times transmission in band i is:
$$(\varepsilon\tau)_i(CW) = \int_{\lambda(i)_a}^{\lambda(i)_b} R^*_\lambda \varepsilon_\lambda \tau_\lambda(CW) d\lambda,$$
6. Store $\tau_i(CW)$ and $(\varepsilon\tau)_i(CW)$ in a table which can be read quickly.

2.5. Finding the optimum water temperature

Suppose we have measured radiances $L_{m,i}$ for $M \geq 3$ channels and would like to retrieve the water temperature $T_w(i)$, columnar water vapor CW and effective atmospheric temperature T_a. A necessary but not sufficient criterion for a good atmospheric correction is that the standard deviation of the estimated water temperatures $\hat{T}_w(i)$ is minimized. The algorithm implemented has the following steps:

1. Find a pixel with water in the image.
2. For a selected atmosphere k (e.g. mid-latitude winter, US standard, ...):
   (a) Compute the estimated water temperature in channel i using:
$$\hat{T}_w(i) = B_i^{-1}\left[\frac{L_m(i) - B_i(T_a)[1-\tau_i(CW)]}{(\varepsilon\tau)_i(CW)}\right],$$
   over a range of CW and T_a, until the estimated water temperatures $\hat{T}_{w,i}$ are most similar, i.e. minimize the standard deviation (STDEV) for a set of spectral channels i or mathematically: $\sigma_k = STDEV(\hat{T}_{w,i}) = minimum$.
   (b) Use the columnar water amount CW_{opt} and the effective atmospheric temperature $T_{a,opt}$ which minimize $STDEV(\hat{T}_{w,i})$ for the atmospheric correction of the radiance in all other water pixels.
3. Select the standard atmosphere k which is the best fit based on the smallest standard deviation σ_k of estimated water temperatures $\hat{T}_{w,i}$.

In Figure 2 we show the 3d surface of the standard deviation σ_k. In the left plot in Figure 3 we plot the columnar water vapor and standard deviation which for a fixed atmospheric temperature is a minimum. The atmospheric temperature which minimizes the standard deviation is 281 K with a columnar water vapor of 4.57 g/cm^2. On the right plot the mean brightness temperature of 4 spectral channels (KLMN) is shown with stars. Where the standard deviation is minimal the brightness temperature curves of individual channels cross.

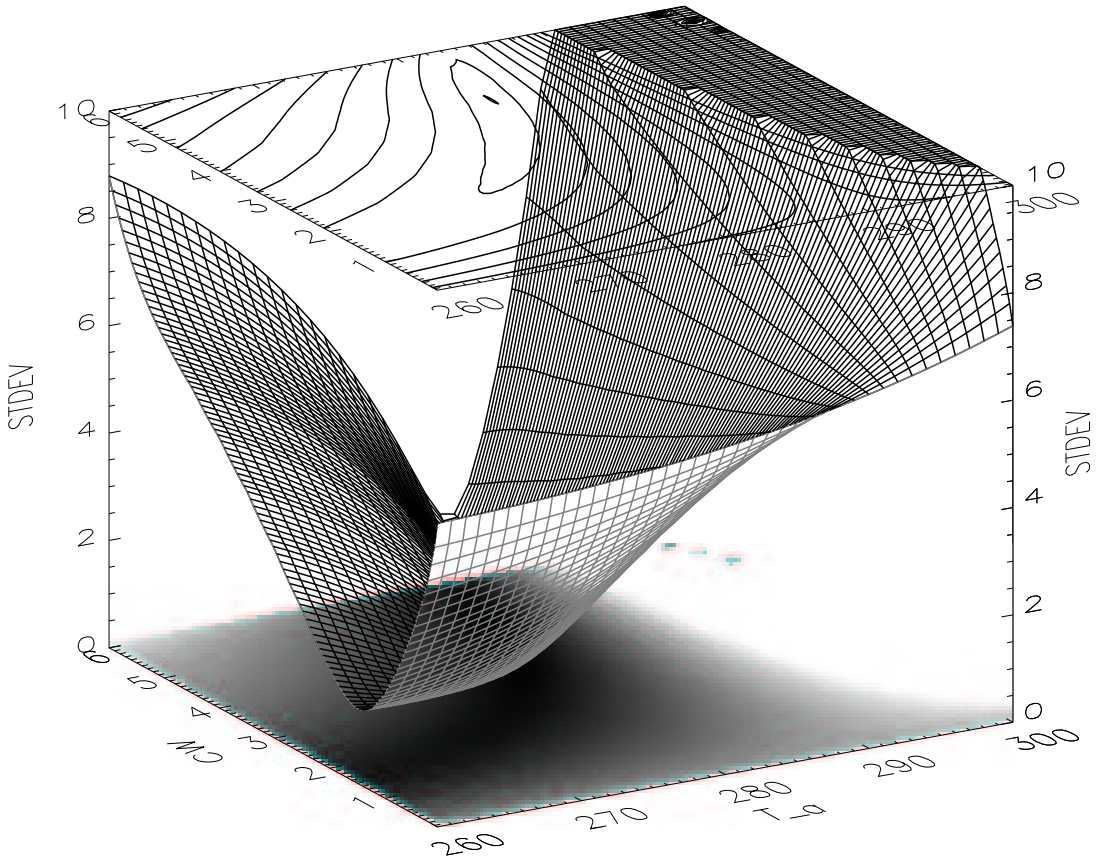

Figure 2. Standard deviation of the retrieved temperatures for channels KLMN as a function of effective atmospheric temperature T_a and columnar water vapor CW.

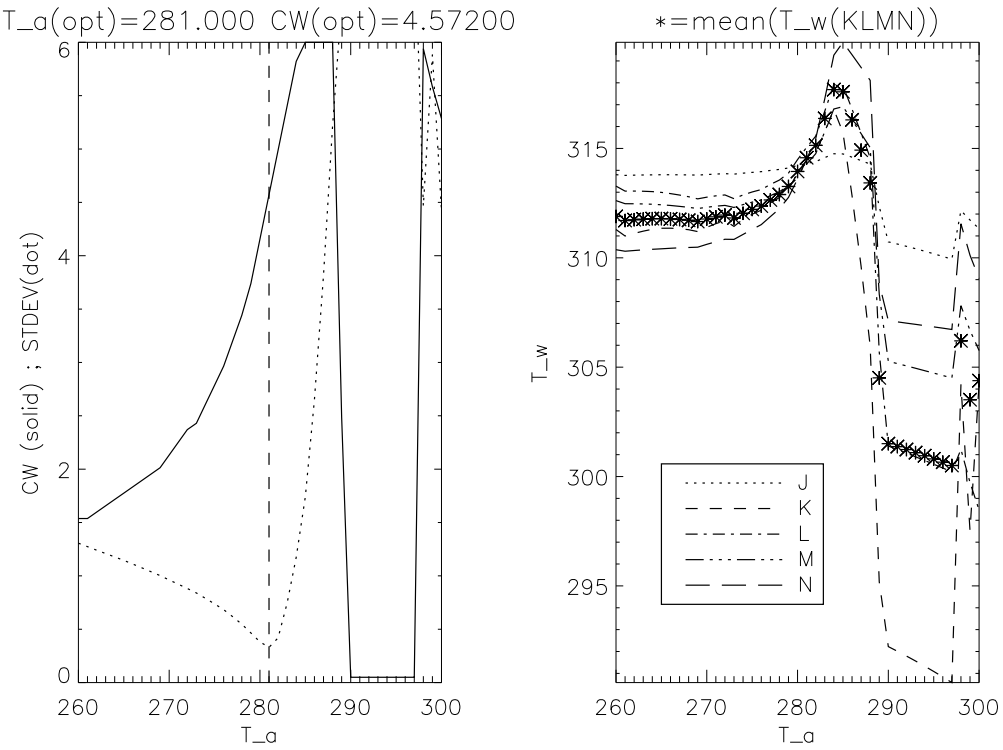

Figure 3. Standard deviation of the retrieved temperatures for channels KLMN as a function of effective atmospheric temperature T_a and columnar water vapor CW.

Blackbody temperature in K					
Channel	250.000	275.000	300.000	325.000	350.000
J (3.5-4.1 μm)	0.0396812	0.160335	0.499058	1.30691	2.98686
K (4.87-5.07 μm)	0.356723	1.02618	2.47562	5.21626	9.88215
L (8-8.4 μm	2.88580	5.45944	9.29222	14.5840	21.4777
M (8.4-8.85 μm)	3.16871	5.80950	9.63493	14.7947	21.3864
N (10.2-10.7 μm)	3.88588	6.42711	9.78808	13.9924	19.0352

Table 1. Band average radiance in $W/(m^2\ \mu m\ sr)$ as a function of spectral channel and blackbody temperature.

2.6. Methods to convert from band averaged radiance to temperature and back

An interesting implementation detail is how we converted from band averaged radiance to temperature and back. The approach we chose is based on ground calibration data of MTI optical assembly looking at 5 black bodies in a vacuum tank (Bender & Atkins, 2000). The radiances of the blackbodies were computed using an average spectral response function over all pixels. In Table 1 we list the band averaged radiances for 5 spectral channels and 5 black body temperatures.

Several interpolation schemes were considered:

1. A quite natural way is to fit the temperature using $T(L_i) = a_i(L_i)^{b_i}$, where $a_i = 335.01, 335.13, 254.18, 246.34, 227.38$ and $b_i = 0.078379, 0.10109, 0.16729, 0.17586, 0.21137$. Unfortunately this method creates systematic errors of up to 2 K compared to a spline interpolation which fits each calibration point exactly.

2. Converting from x =radiance to y =temperature can be done by spline interpolation using the 5 temperatures. We found however that the spline interpolation from temperature to radiance produced large oscillations of up to 3 K amplitude in channel J, 2 K in K and less than 0.4 K for L, M and N.

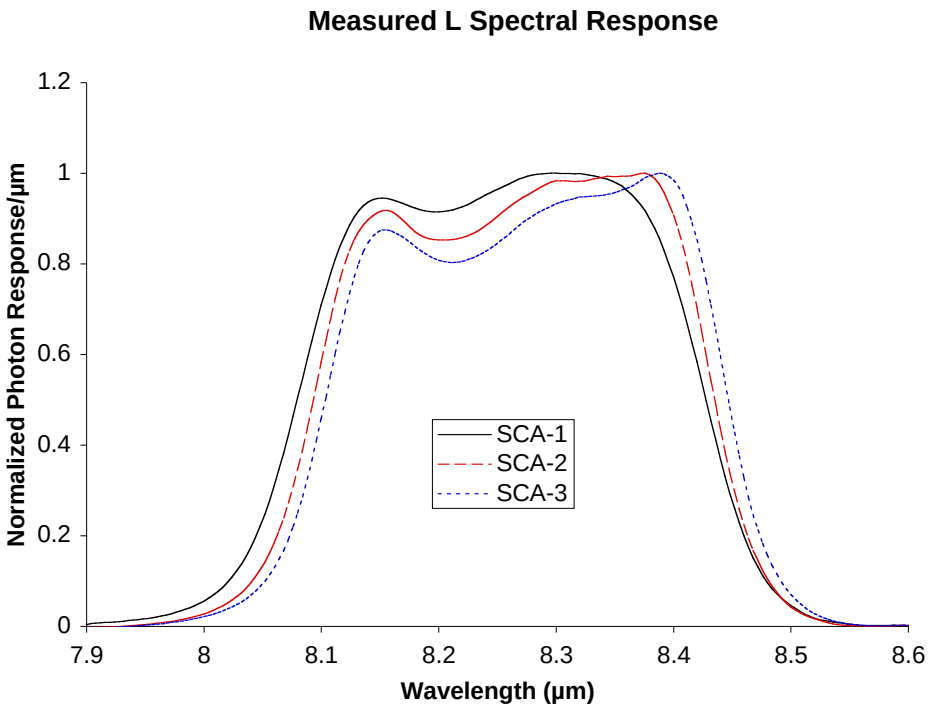

Figure 4. Average spectral response for sub-chip assemblies 1, 2 and 3 for channel L.

3. A better approach is to first increase the number of temperatures and radiances using x =radiance and y =temperature and second perform a spline interpolation with x =temperature and y =radiance. This will result in negligible temperature errors going from radiance to temperature and back.

2.7. The effect of spectral response shifts on the band-average atmospheric transmission

MTI's ground radiometric calibration was based on filter functions which were measured at room temperature at nadir incidence. Using a model these filter functions were converted to pixel dependent filter functions at the actual incidence angles for a cone of light from a $f3.5$ optical system at 75 K. These calculated spectral filters F_λ were used to define R^*_λ assuming that the detector response D_λ was flat through the spectral range of interest. Measurements of all pixels spectral response R^*_λ performed with a monochromator were made when the MTI payload was in the calibration tank. The spectral response of the monochromator itself was later calibrated using special calibrated single detectors. At launch and for several months on orbit we had only 9-point calibrations similar to Table 1 for each sub-chip assembly (SCA) to convert radiance into brightness temperature and back. Using these calibrations we noticed discontinuities across the 3 SCA's in bands K and L which we first attributed to calibration errors caused by a potential obscuration during the ground calibration. Only when data from the door which acts as a calibration target and moon looks were analyzed it was found (Bender & Atkins, 2000) that the discontinuities were not as large as when we observed targets on the Earth. This led us to suspect that small spectral shifts of bands K and L, which lie near water vapor and other gas absorption features might be responsible for these discontinuities. In Figure 4 we show the spectral shifts between SCA's for channel L.

When the pixel dependent new spectral responses became available, a program was written to compute the band average transmission for various atmospheres and view angles for each SCA, see Figure 5. Indeed we found differences of up to one percent between the SCA's as is shown in Figure 6 and RMS variations of up to 0.25 % within a single SCA, see Figure 7. We believe that the pixel and SCA dependent spectral response shifts are responsible for the residual errors we observe between retrieved water temperatures and in-situ measurements.

2.8. Recipe for a temperature/emissivity separation algorithm

The atmospheric correction can be used to retrieve an emissivity over non-water pixels with the following assumptions:

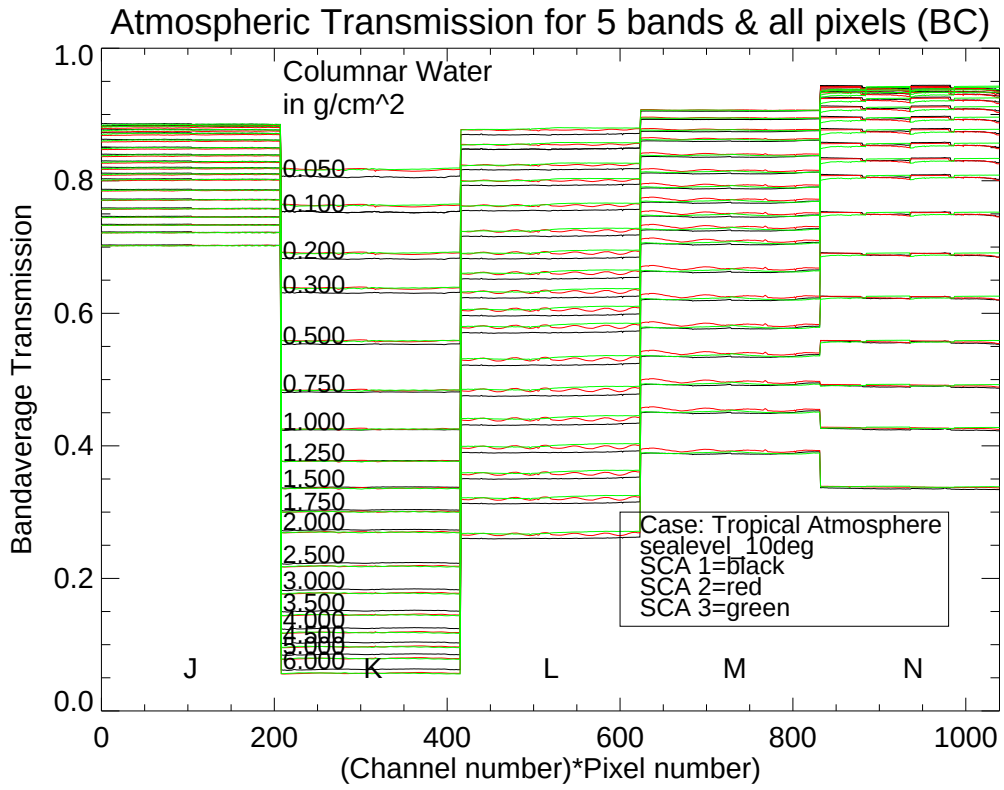

Figure 5. Atmospheric transmission as a function of pixel location and SCA.

1. The multi-spectral instrument has a channel j for which most emissivities reach a similar level, e.g. around 11.5 μm many natural surfaces have emissivities between 0.95 and 0.97 (Salisbury and D'Aria, (1992)).
2. The atmosphere is homogeneous over the scene.

Thus the algorithm we implemented looks like this:

1. Determine the atmospheric parameters over water surfaces.
2. Apply the atmospheric correction to all pixel radiances:

$$L_{c,i} = \frac{L_{m,i} - B_i(T_{a,opt})[1 - \tau_i(CW_{opt}])}{(\varepsilon\tau)_i(CW)}.$$

3. Determine the skin temperature in the channel j assuming a fixed emissivity $\varepsilon_{0,j}$:

$$T_{s,j} = B_i^{-1}\left[\frac{L_{c,j}}{\varepsilon_{0,j}}\right].$$

4. Compute the emissivities in the other channels $i \neq j$ by:

$$\varepsilon_i = \frac{L_{c,i}}{B_i(T_{s,j})}.$$

This algorithm has been implemented and used on MTI data but we are not yet certain about its accuracy.

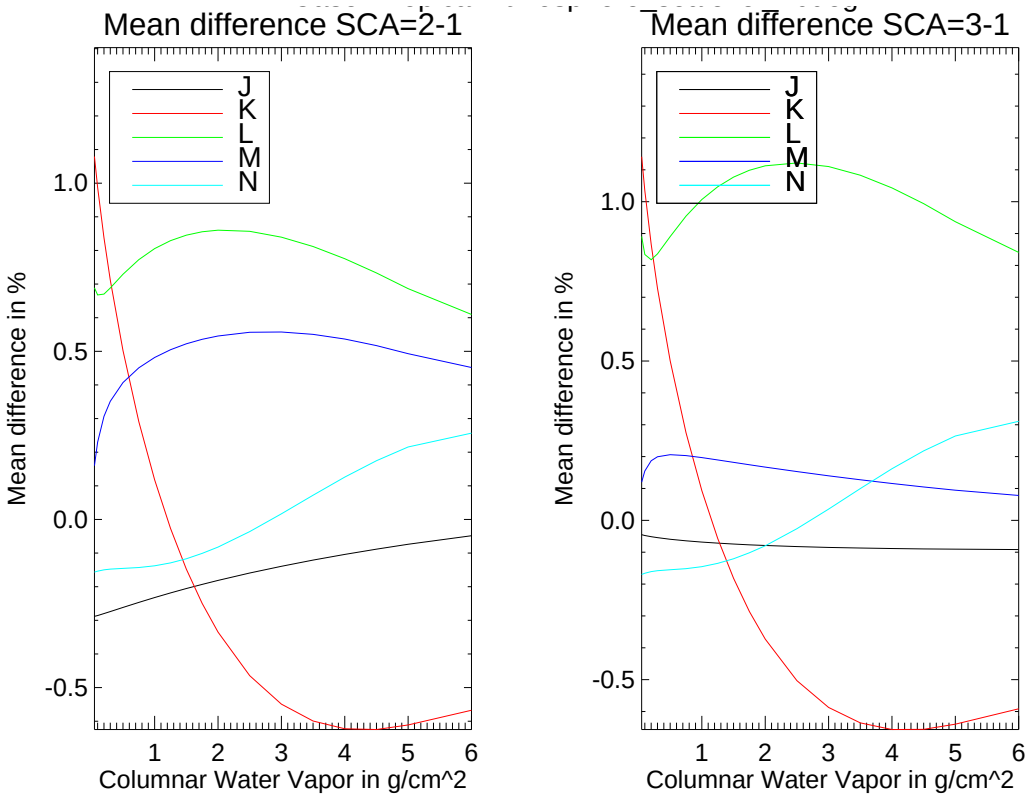

Figure 6. Atmospheric transmission difference between SCA's as a function of water vapor.

3. Results

The physics based water temperature retrieval was applied to radiometric calibrated multi-spectral data from MTI over a variety of water temperatures and atmospheric conditions. Results from two datasets will be discussed here:

Site A: The Squaw Creek Reservoir in Texas is located in a hot and humid area where the bulk water temperatures range from 34^o to 40^o C during the observation period.

Site B: The Crater Lake in Oregon which is a very deep lake (600 m) at 1800 m altitude with temperatures ranging from 5^o to 17^o C over the observation period.

Both locations had precision sensors in place to measure the bulk water temperature. Weather data from the Global Data Assimilation System (GDAS) was used for site A to retrieve the effective atmospheric temperature and columnar water vapor for the dates when we obtained cloud free imagery.

We used 4 out of 5 thermal channels from MTI since one of the channels is contaminated by solar scattered light (J from 3.5-4.1 μm) during the day. We also experimented with subsets of 3 channels out of the 4 thermal channels, e.g. KLM, LMN, KMN to see if the RMS temperature error could be reduced. To retrieve the actual water temperature we experimented with averages over 3 and 4 channels and single channels as shown in Figure 8 for site A. Results for site B are shown in Table 2. Note that SRTC's measurement was not available for the first day and that it was partially cloudy on the second day. If the second day is omitted the mean difference between OSU and MTI data is 1.1 K and the variance is 0.76 K. In Figure 9 we show the comparison of atmospheric parameters derived from GDAS and the quantities derived using the physics based water temperature retrieval. The observed differences show that using GDAS data for atmospheric correction could introduce some errors assuming that the sensor derived atmospheric parameters are more accurate.

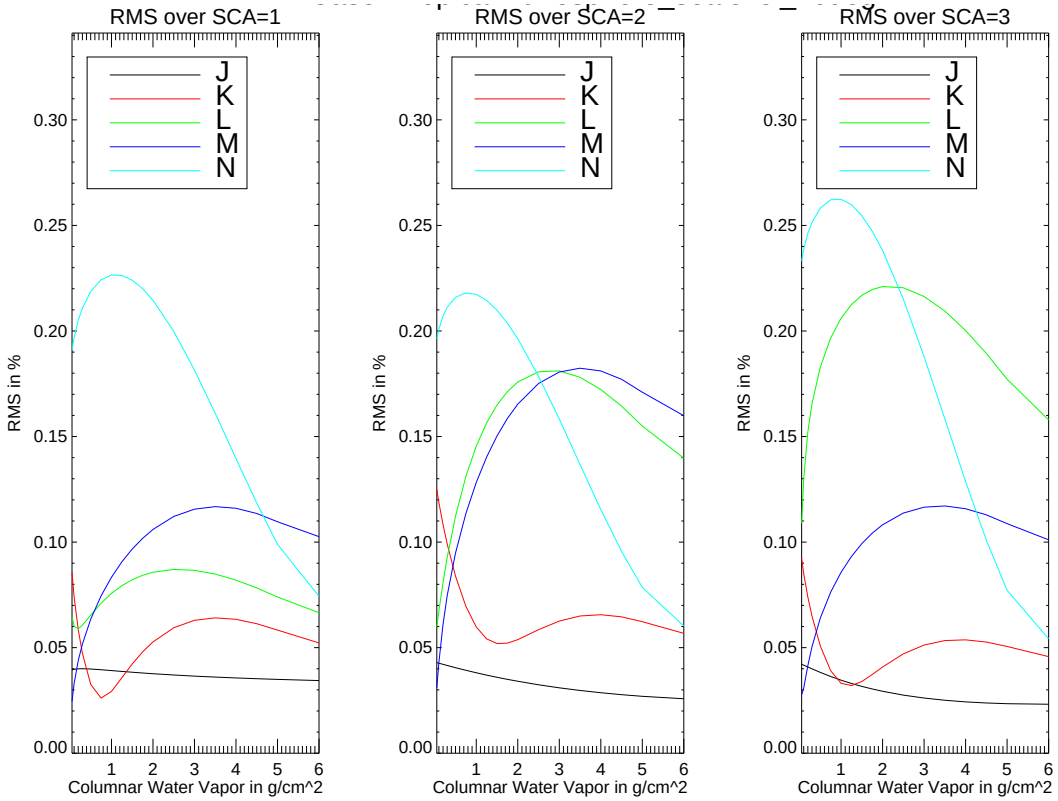

Figure 7. RMS of transmission within a SCA as a function of water vapor.

	Day				
Source	1	2	3	4	5
OSU	5.5	16.45	16.01	15.73	13.51
SRTC	NA	17.02	16.08	16.1	13.43
MTI	7.5	12.3	16.4	16.29	14.98

Table 2. Retrieved skin water temperature versus measured bulk water temperature for Crater Lake, Oregon. The mean difference to MTI retrievals was 0.05 K for OSU data and -0.66 K for SRTC data. The variance to MTI retrievals was 2.44 K for OSU and 2.72 K for SRTC.

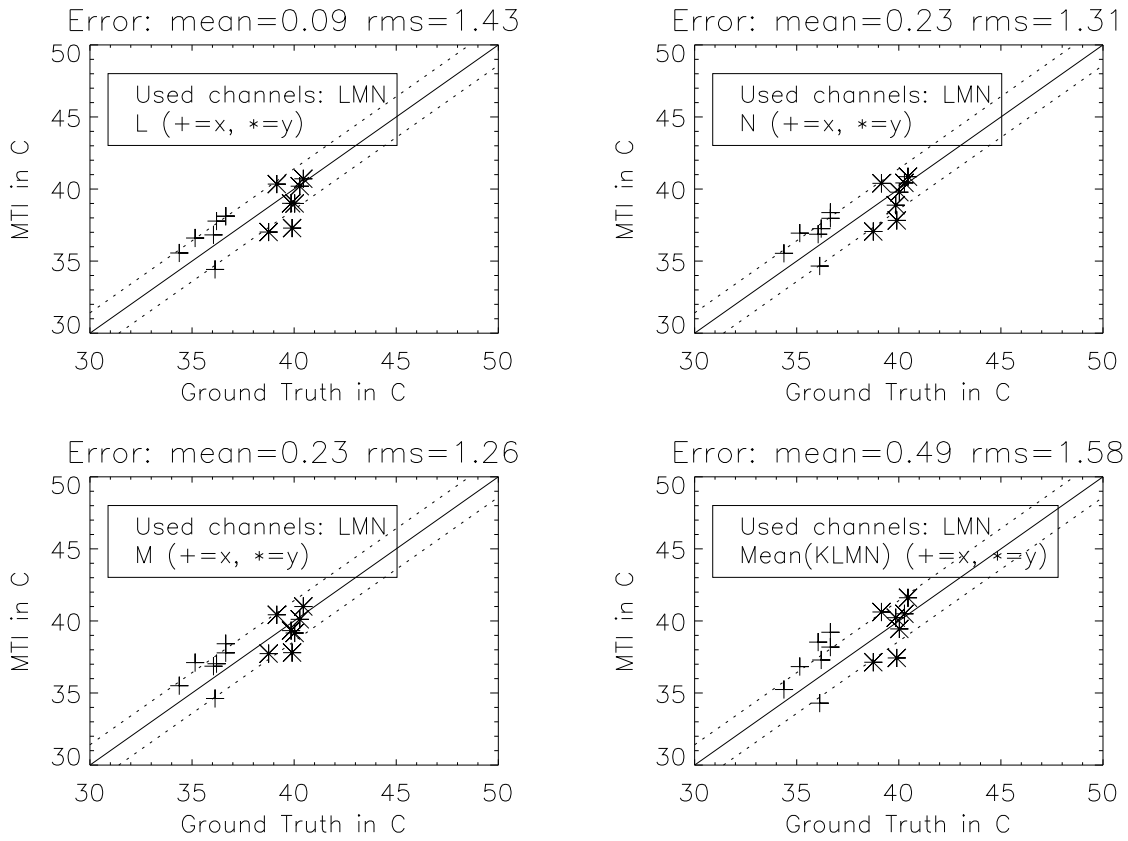

Figure 8. Scatter plots with retrieved skin water temperature versus measured bulk water temperature for 2 sensor locations x and y and site A.

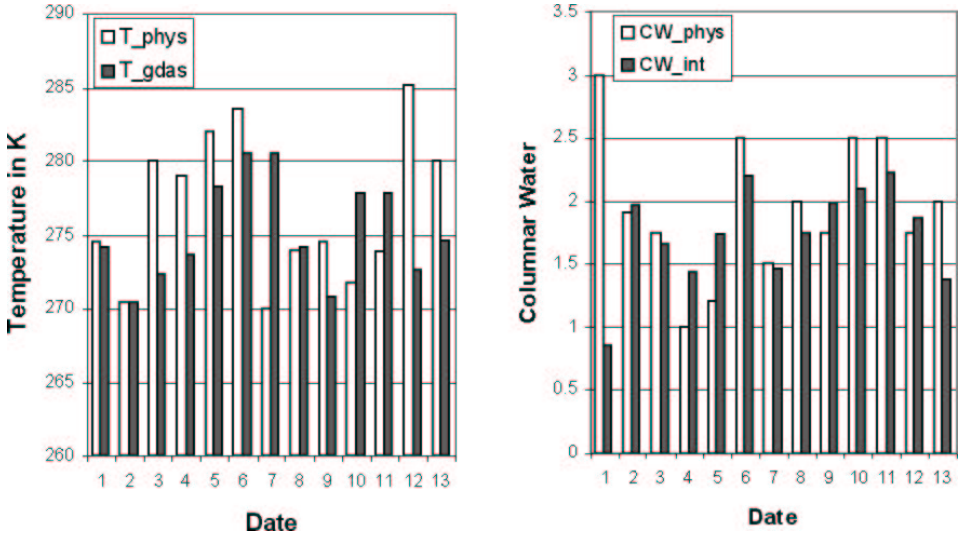

Figure 9. Comparison of physics based retrieved atmospheric parameters with Global Data Assimilation System (GDAS) data. The root mean square error $RMSE(T_a(phys) - T_a(gdas))$ is 5.06 K and for the water vapor $RMSE(PW(phys - PW(gdas)$ = 1.21. For one of the dates (7) no water vapor or atmospheric temperature could be retrieved.

4. Conclusions

We find that the method proposed in a theoretical paper in Borel et al (1999) works on actual data from MTI. The absolute temperature error is somewhat larger than predicted because some of the MTI bands lie close to strong atmospheric absorption features where due to small spectral shifts in the filters can change the band averaged transmission by up to one percent which results in about 1 K temperature error.

Future enhancements of the code will include generation of more realistic atmospheric transmission and path radiance data using GDAS derived atmospheric profiles in MODTRAN calculations. We expect the atmospheric transmission and path radiance to be more realistic because the width and depth of gas and water vapor absorption lines are strongly temperature dependent, an effect which is not adequately modeled using the current standard atmospheres.

In conclusion we find that the physics based retrievals of water temperatures is accurate to within +/-1.5 to 2 K. The retrieved water vapor amounts and effective atmospheric temperatures differ to about 1.2 $g/cm^(- 1$ and 5 K for the cases we compared from GDAS data which could lead to better water temperature estimates assuming that the sensor derived atmosphere is more accurate.

Acknowledgements

Many people at Los Alamos National Laboratory, Sandia National Laboratories and Savannah River Technological Center and other partners in industry and academia contributed to the success of the MTI project. At LANL we acknowledge the leadership and encouragement of the project leaders Paul Weber and John J. Szymanski, and the tremendous efforts by Steve Bender and many others to get a well calibrated instrument into space. This work was performed with financial support from the Department of Energy under contract W-7405-ENG-36. Part of this study was also supported by a grant from NASA HQ to study temperature retrievals in complex environments (NASA W-19,324).

References

Bender, S.C., Atkins, W.H., *personal communication*, 2000.

Borel, C.C., W.B. Clodius, J.J. Szymanski,and J. Theiler, Comparing robust and physically based sea surface temperature retrievals for high resolution, multi-spectral thermal sensors using one or multiple looks, *SPIE conference 3717 on Algorithms for Multi-spectral and Hyperspectral Imagery*, Orlando, 5-9 April, 1999.

Cox, C. and W. Munk, Measurements of the roughness of the the sea surface from photographs of the sun's glitter, *JOSA*, 44, 838-850, 1954.

Henderson, B. G., J. Theiler and P. Villeneuve, The polarized emissivity of a wind-roughened sea surface: a Monte Carlo model, *Rem. Sens. Envir.*, accepted for publication, 2001 or *LA-UR-97-14*.

Irvine, W. M. and J. B. Pollack, Infrared optical properties of water and ice spheres, *Icarus*, 8, 324, 1968.

Salisbury, J. W. and D. M. D'Aria, Emissivity of terrestrial materials in the 8-14 μm atmospheric window, *Remote Sens. Environ., 42*, 83-106, 1992.

Theiler, J. and B. G. Henderson. A Geometrical Constraint on Shadowing in Rough Surfaces, *Proc. SPIE*, 3122 271-279, 1997.

Pierson, W.J. and L. Moskowitz, A proposed spectral form for fully developed wind seas based on the similarity theory of S.A.Kitaigorodskij, *JGR 69*, 5181, 1964.

Preisendorfer R. and C.D. Mobley, Albedos and glitter patterns of a wind-roughened sea surface, *J. Phys. Ocean.* 16(7), 1293-1316, 1986.